Journal of Alloys and Compounds 490 (2010) 241–246

Contents lists available at ScienceDirect

Journal of Alloys and Compounds

journal homepage: www.elsevier.com/locate/jallcom

Mechanistic insight of electrochemical reduction of Ta_2O_5 to tantalum in a eutectic $CaCl_2$–NaCl molten salt

Qiu-shi Song[a], Qian Xu[a,*], Xue Kang[a], Ji-hong Du[b], Zheng-ping Xi[b]

[a] School of Materials Science and Metallurgy, Northeastern University, Shenyang 110004, China
[b] Northwest Institute for Non-ferrous Metal Research, Xi'an 710016, China

ARTICLE INFO

Article history:
Received 16 April 2009
Received in revised form
30 September 2009
Accepted 30 September 2009
Available online 6 October 2009

Keywords:
Electrochemical reduction
Tantalum
Tantalum pentoxide
Particle morphology
X-ray diffraction

ABSTRACT

An investigation into the reaction pathway of the electrochemical reduction of Ta_2O_5 to tantalum in a eutectic $CaCl_2$–NaCl molten salt has been performed in order to better understand the reaction mechanism of the electro-deoxidation process. Partially reduced samples were obtained by interrupting the reduction process after different reaction times at 1123 K, and examined by XRD, SEM and EDX analysis. The results reveal that the reduction process from Ta_2O_5 to Ta undergoes several intermediate phases, such as Ta_2O_5·0.5CaO, Ta_2O_5·2CaO, and Ta_2O_5·4CaO. The particle morphology in the cathode changed with the various phase transformations. The CaO concentration in the $CaCl_2$–NaCl melt seems to affect the particle size of nodular-shaped tantalum powder products.

1. Introduction

Tantalum is widely used because of its properties of strong corrosion resistance, high melting point, good ductility and heat conductivity, etc. However, the major use for tantalum, as tantalum metal powder, is in the production of tantalum capacitors, which have very high capacity relative to their small volumes. The dielectric is formed from a very thin anodized layer of tantalum pentoxide. Tantalum powder can be industrially produced by sodiothermic reduction of K_2TaF_7 in the KCl–NaCl–NaF molten salt. In this process K_2TaF_7 is made from tantalum oxide ores, and then was reduced to Ta at high temperatures (>1000 K) using sodium. However, it is considered as a complex, expensive, and environmentally polluting process [1–3], but, in recent years, some new processes have been developed as promising methods to replace the fluoride-based process someday [1,4–16]. Metallothermic and electrochemical reduction are two important processes carried out in molten salts, from which many new metallurgical routes were derived, such as FFC [6,7], EMR [9], PRP [10,11] and SOM [15,16]. The FFC process is a method to obtain metals and alloys by direct electro-deoxidation of their respective oxides or mixtures of oxides in chloride-based molten salts, which should be a much easier, less expensive and more environmentally friendly way [2,17–21]. Many metals and alloys have been produced by using this process, such as Nb [17,22–24], Ta [2,8,25], Ti [6,20,21,26], Al [27], Nb–Sn [18], Ni–Ti [28], Fe–Ti [29], Ce–Ni [30] and La–Ni [31,32]. Additionally, the possible mechanism for the electro-deoxidation process has been discussed [20–21,23,33,34], and some models also has been applied to understand the process [35,36].

The metallothermic or electrochemical reduction of Ta_2O_5 has been achieved in $CaCl_2$-based molten salts without any fluoride [6,9,12,13]. In particular, as a medium for the reactions, the molten $CaCl_2$ can enhance the reduction because the product CaO, produced at the reaction interface, can dissolve into the $CaCl_2$ melt [4,5,13]. Furthermore, the CaO in the molten $CaCl_2$ can play an interesting role on the reduction of Ta_2O_5, which can affect the morphology of tantalum powder prepared for the calciothermic reduction [4,13], and form calcium tantalates as the intermediates for the FFC process [2,33,34]. Greater understanding of CaO reactions during the reduction in the molten $CaCl_2$–NaCl will be useful in comprehending the mechanism of the FFC process.

The objective of this work has been to gain a greater insight into the reaction between Ta_2O_5 and the CaO in the molten $CaCl_2$–NaCl which occurs in the course of the electrochemical reduction of Ta_2O_5 to tantalum in the FFC process. It is intended to understand the electrochemical reductions of Ta_2O_5 in the melt of $CaCl_2$–NaCl in order to better control and optimize experimental parameters, which may be critical for successful industrialization.

* Corresponding author.
E-mail address: qianxu201@mail.neu.edu.cn (Q. Xu).

0925-8388/$ – see front matter © 2009 Elsevier B.V. All rights reserved.
doi:10.1016/j.jallcom.2009.09.168

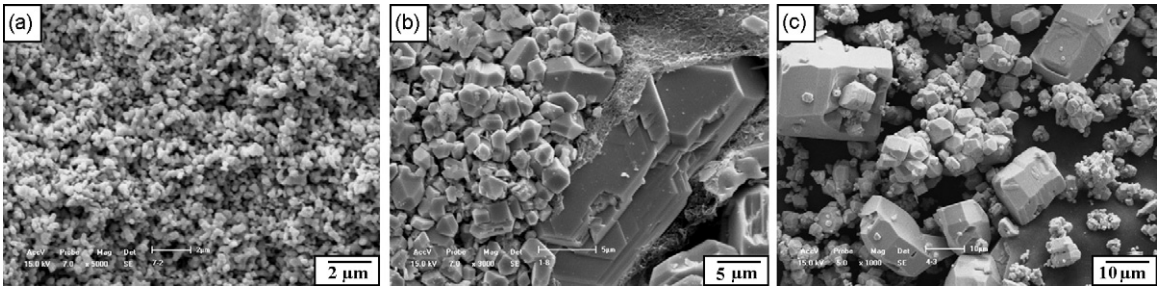

Fig. 1. SEM images of (a) the Ta_2O_5 pellet sintered at 1273 K for 4 h; (b) the sample immersed in the $CaCl_2$–NaCl melt with about 1 mol% CaO for 7 h; (c) the sample immersed in the $CaCl_2$–NaCl melt for 10 h.

2. Experimental

The Ta_2O_5 powder was of 99.99% purity and purchased from Sino-pharm Chemical Reagent Co. Ltd. Other chemicals in this study were of analytical grade. 1.5 g of Ta_2O_5 powder was weighed and compacted into cylindrical pellets (15 mm in diameter and 2.3 mm in thickness) under 17 MPa, and then the oxide pellets were sintered at 1273 K in air for 4 h. A eutectic mixture of $CaCl_2$ and NaCl was first thermally pre-dried, then melted in an alumina crucible and served as the electrolyte. The electrochemical experiments were conducted at 1123 K under an atmosphere of dried argon. The electrolysis temperature is about 346 K higher than the eutectic temperature of the $CaCl_2$–NaCl binary system, therefore the eutectic melt has a high mobility and conductivity, which are favorable for the electrolysis.

For some experiments, about 1 mol% of CaO was added into the melt. The sintered Ta_2O_5 pellets served as the cathode, and a graphite rod as the anode, both were attached to Kanthal wires which acted as the current collectors. The experimental apparatus used here was similar to that described in the literature [8,23,25].

A voltage of 2.8 V was applied between the cathode and anode for the predetermined times. The partially and totally reduced samples were obtained by stopping the electrochemical reduction at any time from 0.5 h to 24 h. In order to get the chemical behavior of sintered Ta_2O_5 pellets in the electrolyte melt with and without the addition of CaO, the pellets were immersed in the melts for the times from 6 h to 10 h with no cathodic polarization. After the simple immersion and electrochemical reduction, respectively, the recovered samples were washed in deionized water and dried in ambient air at room temperature. Each of the reduced or immersed pellets was separated into several pieces for examination. Phase analysis of the samples was carried out with a D/Max-2500PC X-ray diffractometer with Cu-Kα radiation, and the morphology was investigated by means of a SSX-550 scanning electron microscope (SEM) equipped with energy-dispersive X-ray analysis.

3. Results and discussion

3.1. The chemical reactions of Ta_2O_5 with CaO in the $CaCl_2$–NaCl melt

Fig. 1a shows the SEM image of a porous Ta_2O_5 pellet sintered at 1273 K for 4 h. The pellet typically contains particles of about 0.5 μm in diameter with an open porosity of 30–35%. The chemical behavior of Ta_2O_5 in the $CaCl_2$–NaCl melt with an addition of about 1 mol% CaO was investigated by submersing the oxide pellets into the melts for 6 h and 7 h, respectively, and their XRD patterns are both shown in Fig. 2a–c together with the XRD pattern of the sintered Ta_2O_5 sample. The sample quenched after being immersed for 6 h is characterized by the overwhelming presence of Ta_2O_5·CaO. As the immersing time increases, Ta_2O_5·2CaO occurs as well as Ta_2O_5·CaO in the sample immersed for 7 h. Meanwhile, the samples in the $CaCl_2$–NaCl melt with no addition of CaO for 6, 7 and 10 h were also composed of calcium tantalates as well, which typical XRD patterns are shown in Fig. 2d–f. In general, there is a small amount of CaO as an impurity in the $CaCl_2$–NaCl melt since calcium chloride can absorb some moisture in ambient air and form CaO from its derivatives like calcium hydroxide after being thermally pre-dried and heated up to 1123 K. But, the concentration of CaO should be lower than that in the $CaCl_2$–NaCl melt with about 1 mol% CaO added. That is the probable reason for formation of CaO–Ta_2O_5 compounds in the $CaCl_2$–NaCl melt with no addition of CaO. The reaction shown in Eq. (1) could occur spontaneously and successively in the $CaCl_2$–NaCl melt with some CaO at 1123 K.

$$n\mathrm{CaO} + \mathrm{Ta_2O_5} \rightarrow \mathrm{Ta_2O_5} \cdot n\mathrm{CaO} \quad (n = 0.5, 1, 2, 4) \tag{1}$$

Moreover, there are stable calcium tantalates observed in Ta_2O_5–CaO binary phase diagram [37]. The predominant calcium tantalate formed in the $CaCl_2$–NaCl melt is Ta_2O_5·0.5CaO in the sample which was immersed for 6 and 7 h, and a little of Ta_2O_5·CaO was found in the sample for 10 h. Although the duration of its immersion in the melt is longer than that of the samples in the $CaCl_2$–NaCl melt with about 1 mol% CaO, the number of CaO incorporated into one Ta_2O_5 unit on average is smaller. Therefore, it can be deduced that the number of CaO included per Ta_2O_5 unit for the calcium tantalate seems strongly dependent on the concentration of CaO in the $CaCl_2$–NaCl melt.

Fig. 1b shows the morphology of the Ta_2O_5 pellet which was immersed in the $CaCl_2$–NaCl melt with about 1 mol% CaO for 7 h, and then quenched and washed in water. There are larger, lath-shaped particles in the interior region of the pellet, in which the molar ratio of Ta to Ca is about 2:1 according to the EDX analysis together with its SEM image. These are expected to be the compound of Ta_2O_5·CaO by considering of its XRD analysis shown in Fig. 2c. There are also relatively smaller, cubic particles in the outer region of the same pellet, where the ratio is close to 1:1 by EDX analysis. These are the compound of Ta_2O_5·2CaO, which was deduced by considering of their XRD and EDX analysis. There is a clear boundary between the inner and outer region, marked by a diffuse reaction front moving into the pellet from its surface. Probably, Ta_2O_5·2CaO can be formed in the outer region where CaO in the melt has diffused through the channels of open porosity in the sample. Elsewhere, the CaO percolation has been less effective, and

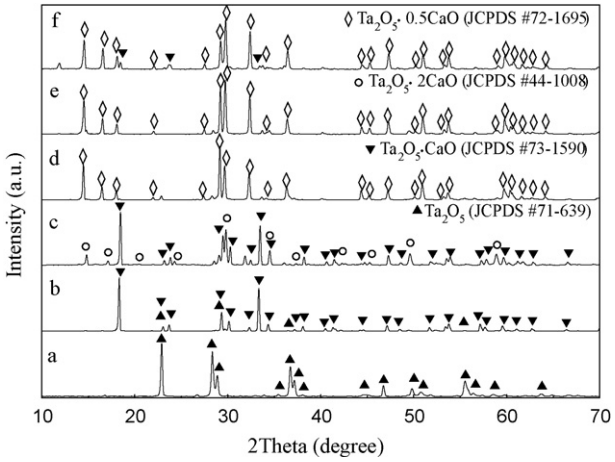

Fig. 2. XRD patterns of (a) the Ta_2O_5 sintered pellet; (b) and (c) the samples immersed in the $CaCl_2$–NaCl melt with about 1 mol% CaO for 6 h and 7 h, respectively; (d)–(f) the samples immersed in the $CaCl_2$–NaCl melt for 6 h, 7 h and 10 h, respectively.

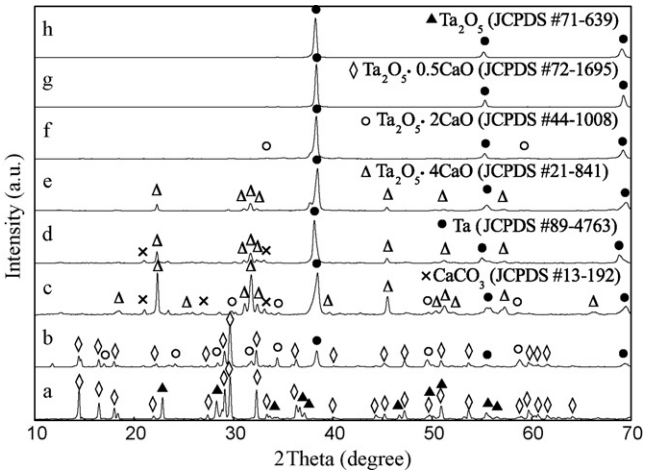

Fig. 3. XRD patterns of the samples electro-deoxidized in the $CaCl_2$–NaCl melt with about 1 mol% CaO for various times. (a) 0.5 h, (b) 1 h, (c) 2 h, (d) 4.5 h, (e) 5.5 h, (f) 10 h, (g) 13 h and (h) 24 h, respectively.

Ta_2O_5·CaO has been formed in the inner region since the amount of CaO is in short supply, and the local concentration of CaO was lower in the inner region of the pellet. Similar effects probably occurred for the samples in the melt without the addition of CaO for 10 h though the quenched sample was broken up after being washed in water and its integrity was not maintained. Fig. 1c shows its SEM image. The particles should be the compound of Ta_2O_5·0.5CaO, which was identified by its XRD pattern in Fig. 2f. The calcium tantalates in this study exhibit a strongly faceted morphology as shown in Fig. 1b and c. The particle size of Ta_2O_5·0.5CaO can reach up to 20 μm shown in Fig. 1c, which is about 40 times bigger than that of the original grains in the Ta_2O_5 pellet. The atomic structures formed from corner-, edge- and face-sharing TaO_6 octahedra while Ca^{2+} ions were located in interstitial sites among the octahedra. The greater amount of CaO that was incorporated per Ta_2O_5 unit, the greater the number of O atoms that go to the TaO_6 octahedron arrays. Therefore, the number of bridging oxygen (BO) decreases and the number of non-bridging oxygen (NBO) increases in the TaO_6 octahedron arrays so that the more complex and bigger networks of TaO octahedra were broken up into simpler and smaller ones. CaO behaves here as a network modifier.

3.2. The electrochemical reduction of Ta_2O_5 in the $CaCl_2$–NaCl melt with about 1 mol% CaO

The partially reduced tantalum oxide specimens were obtained by interrupting the electrochemical reduction after different reaction times. Fig. 3a–c show the XRD patterns of partially reduced samples in the $CaCl_2$–NaCl melt with about 1 mol% CaO for 0.5 h, 1 h and 2 h, respectively. The sample quenched after electrolysis for 0.5 h consists predominantly of Ta_2O_5 and Ta_2O_5·0.5CaO, the latter is one member of calcium tantalates which are formed by the chemical reactions shown in Eq. (1) as explained previously. Even though electrons were supplied to the tantalum oxide cathode, no tantalum sub-oxides can be identified from the XRD pattern. One of the most likely effects during reduction is the formation of oxygen vacancies in the atomic structures of Ta_2O_5 or Ta_2O_5·0.5CaO. The reaction can be expressed as Eq. (2).

$$Ta_2O_5 \cdot nCaO + x \cdot 2e = Ta_2O_{5-x} \cdot (V_O)_x \cdot nCaO + xO^{2-} \quad (n = 0, 0.5, 2, 4) \qquad (2)$$

The oxygen vacancies, as point defects, exist in Ta_2O_5 or Ta_2O_5·0.5CaO crystal when oxygen atoms within the oxide crystal frequently obtain the electrons from the cathode lead and move into the $CaCl_2$–NaCl melt, leaving behind empty lattice sites. The value of x in Eq. (2) is determined by the concentration of the oxygen vacancies, which should not exceed the maximum that the stable Ta_2O_5·nCaO crystalline lattice can accept. The intrinsic defects Ta'_{Ta} would be produced in the Ta_2O_5·nCaO crystal particles along with charge compensating defects $V_O^{\bullet\bullet}$, which means Ta_2O_5 is partially reduced during the first 0.5 h of the reduction process although Ta_2O_5 and Ta_2O_5·0.5CaO can only be identified for the typical XRD pattern.

Table 1
The molar ratios of Ta to Ca for the region A and B in Fig. 4a, respectively.

Region	Ta:Ca
A	32:8
B	62:1

Fig. 4a is the SEM image of the partially reduced sample for 0.5 h. There were two types of particles classified by their particle sizes. According to their respective EDX analysis shown in Table 1, the molar ratio of Ta to Ca is 32:8 for the region A, which indicated Ta_2O_5·0.5CaO, confirmed by its XRD analysis; while the molar ratio is about 62:1 for the region B, the major phase is Ta_2O_5 as indicated by the small amount of Ca and its XRD pattern.

The sample recovered after about 1 h is mainly composed of Ta_2O_5·0.5CaO and Ta_2O_5·2CaO, and XRD pattern is also shown in Fig. 3b. There is the additional presence of Ta, which is detected from its typical XRD pattern. But no Ta_2O_5 exists as shown by the XRD pattern. It seems that almost all Ta_2O_5, combined with CaO and form calcium tantalates. Fig. 4b shows the morphology of partially reduced sample for 1 h. The EDX analysis was carried out for the regions which are marked as C and D, respectively. The molar ratio of Ta to Ca is 43: 9 for region C, where the major phase should be Ta_2O_5·0.5CaO, while the molar ratio for region D is 22:16, where two phases should be Ta_2O_5·0.5CaO and Ta_2O_5·2CaO. The morphology of the particles in region D reflects the aggregates of the smaller flakes, which was created by the network modifying effects of CaO in the melt on the surface of Ta_2O_5·0.5CaO. When more of the network-modifying CaO is combined with Ta_2O_5, this disintegrates the larger particles of Ta_2O_5·0.5CaO. It should be mentioned that Ta_2O_5·0.5CaO may still exists inside the particles, which leads the molar ratio of Ta to Ca obtained by EDX analysis to be bigger than 1:1 of Ta_2O_5·2CaO for region D.

Fig. 3c also shows XRD pattern of the sample reduced for about 2 h, which comprises basically Ta, Ta_2O_5·2CaO and Ta_2O_5·4CaO, the latter was not found within the sample immersed simply in the melt both with and without the addition of CaO in this study. During further electrochemical reduction, there are two possible streams to enrich the local concentration of CaO within the cathode. First, CaO can be released directly from calcium tantalates through the reaction (3). Second, the oxygen ions released by the reaction (2) can incorporate with Ca^{2+} in the $CaCl_2$–NaCl melt and form more CaO. The enhancement of the local CaO concentration in the melt which percolates the cathode can lead to an increase in the CaO/Ta_2O_5 ratio. The typical peaks of Ta are more dominant compared with those of the samples reduced for 1 h from their XRD patterns, and there is almost no Ta_2O_5·CaO identified since it can incorporate CaO to form Ta_2O_5·2CaO or Ta_2O_5·4CaO. Finally, tantalum is obtained by the reaction (3).

$$Ta_2O_{5-x} \cdot (V_O)_x \cdot nCaO + 2(5-x)e = 2Ta + (5-x)O^{2-} + nCaO \qquad (3)$$

For the whole electrochemical process, no tantalum sub-oxides and their compounds with CaO were observed from the typical XRD patterns. It is probable that Ta_2O_5·nCaO can be reduced to Ta directly without any intermediates in which the oxidation state of

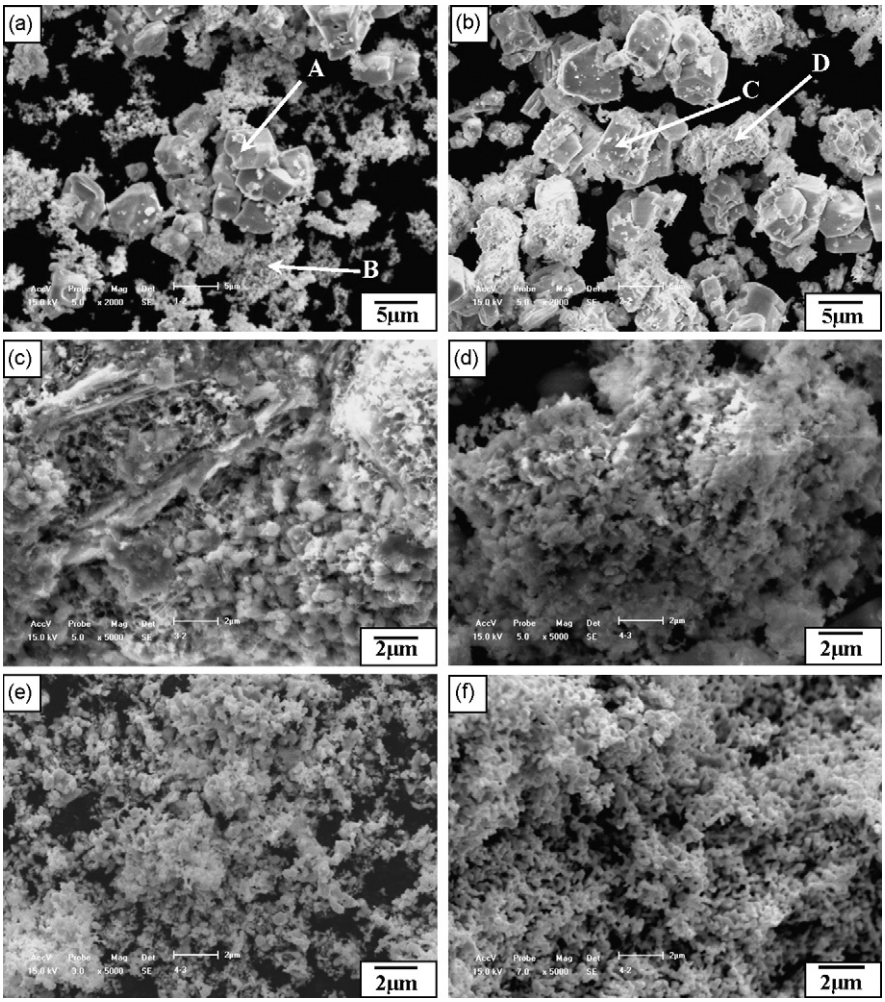

Fig. 4. SEM images of the samples electro-deoxidized in the $CaCl_2$–NaCl melt with about 1 mol% CaO for (a) 0.5 h, (b) 1 h, (c) 2 h, (d) 5.5 h, (e) 10 h and (f) 24 h, respectively.

tantalum atom may be lower than 5. This differs from the reduction pathway of TiO_2 [20,21,33,34] or Nb_2O_5 [22,23] by the FFC process. It is also different from the results of Chen and co-workers [2]. Usually, metals in lower oxidation states can be found during the reduction of TiO_2 in the molten $CaCl_2$ [20,21,33].

Fig. 4c shows the morphology of partially reduced sample for 2 h. The size of most particles in the sample is smaller than 2 μm. The aggregate of particles has an alveolate structure shown in Fig. 4c, which are probably the result of disagglomeration of $Ta_2O_5{\cdot}0.5CaO$ to $Ta_2O_5{\cdot}4CaO$ by combination of more CaO. Therefore, $Ta_2O_5{\cdot}4CaO$ particles are smaller in size than $Ta_2O_5{\cdot}0.5CaO$.

Fig. 3d–f shows the typical XRD patterns of the partially reduced samples for 4.5 h, 5.5 h and 10 h, respectively. The major phase is Ta, and the minor phases are $Ta_2O_5{\cdot}4CaO$, $Ta_2O_5{\cdot}2CaO$ and $CaCO_3$ after 4.5 h electrolysis. The formation of $CaCO_3$ may be because of the use of graphite anode in this study. Carbon dioxide can be generated on the anode during electrolysis, and dissolved in the $CaCl_2$–NaCl melt as CO_3^{2-}. Fig. 4d is the SEM image of partially reduced sample for 5.5 h electrolysis, in which the alveolate structures can be found. Considering its typical XRD pattern, it consists mainly of Ta, and $Ta_2O_5{\cdot}4CaO$ with a smaller particle size. The particles bigger than 5 μm cannot be observed, these are very normal in the sample of 1 h reduction as $Ta_2O_5{\cdot}0.5CaO$. Fig. 4e shows the morphology of the partially reduced sample for 10 h electrolysis. The number of smaller size particles becomes more and more, and some of them are interconnected one another. But the particle size is not uniform probably because the sample is not reduced completely and the calcium tantalates particle size may be bigger.

Fig. 3g–h shows the two typical XRD patterns of the samples reduced for 13 h and 24 h, respectively. Metallic tantalum is the only phase being present in both samples. After undergoing several intermediate phases, such as $Ta_2O_5{\cdot}0.5CaO$, $Ta_2O_5{\cdot}2CaO$ and $Ta_2O_5{\cdot}4CaO$, the starting material Ta_2O_5 was completely reduced to tantalum. During the process of immersion and reduction, only calcium tantalates determined from the XRD patterns and no sodium tantalates are found. Similarly, calcium niobates were formed during the electrochemical reduction of Nb_2O_5 in the $CaCl_2$–NaCl molten salt, while sodium niobates were not observed according the XRD patterns [38,39]. The phenomenon was probably because the calcium tantalates formed were thermodynamically more stable than sodium tantalates in the $CaCl_2$–NaCl melt. Fig. 4f is the SEM image of the sample reduced for 24 h. It shows the uniform particle sizes and similar nodular shapes of the metal tantalum product. One interesting aspect of the Ta particles is that the smaller nodular Ta particles are interconnected to one another, which was also described in the literature [2]. Such structures are considered to be preferable for their application of electronic capacitors.

Fig. 5 is the current vs. time curve of electrochemical reduction experiment in the $CaCl_2$–NaCl melt with about 1 mol% CaO, in which cathode composition was given for various points in time during electrolysis. Based on the explanation of the mechanism put forward above, the current peaks are caused by fast reductions of the cathode with participation of calcium oxide, which lead to

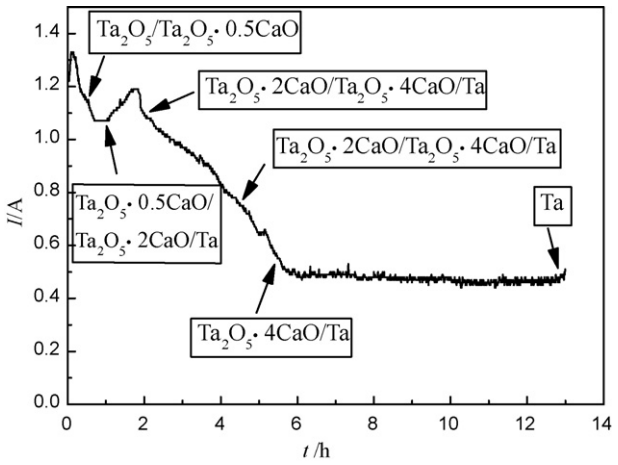

Fig. 5. The current vs. time curve of electrochemical reduction experiment in the $CaCl_2$–NaCl melt with 1 mol% CaO, in which cathode composition was given for various points in time during electrolysis.

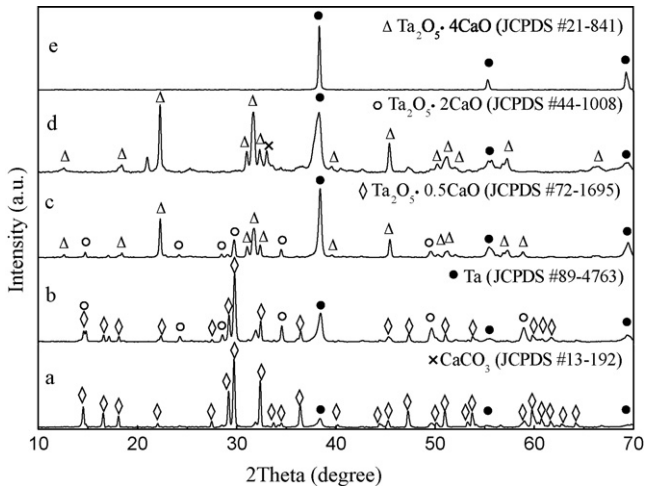

Fig. 6. XRD patterns of the samples electro-deoxidized in the $CaCl_2$–NaCl melt for (a) 0.5 h, (b) 1 h, (c) 2 h, (d) 6.5 h and (e) 12 h, respectively.

the formation of calcium tantalate mixtures. $Ta_2O_5{\cdot}4CaO$ has the most number of CaO per Ta_2O_5 unit among the tantalates, which should have the lowest degree of polymerization for TaO_6 octahedron. It exists until Ta_2O_5 is completely reduced to Ta. During the later stages of the reduction process, while calcium tantalates formation seems to cease, the removal of oxygen from the cathode becomes the dominant process. However, the electronic current now contributes significantly to the overall current, and leads the relatively low overall current efficiency of about 11% for preparation of tantalum with low oxygen contents by the process.

3.3. *The electrochemical reduction of Ta_2O_5 in the $CaCl_2$–NaCl melt*

As mentioned above, there should be some CaO as an impurity in the $CaCl_2$–NaCl melt with no addition of CaO. But the concentration of CaO in the melt is lower than that of the $CaCl_2$–NaCl melt with about 1 mol% CaO added specially. Fig. 6a–c shows the XRD patterns of partially reduced samples in the melt for 0.5 h, 1 h, and 2 h, respectively. Ta had already been detected by XRD analysis for partially reduced sample for 0.5 h, while the characteristic peaks of Ta_2O_5 were not found. The major phase is $Ta_2O_5{\cdot}0.5CaO$, similar to the sample in the melt with about 1 mol% CaO. During the electrochemical reduction, $Ta_2O_5{\cdot}2CaO$ and $Ta_2O_5{\cdot}4CaO$ can be formed successively, which are detected from the XRD patterns of sample reduced for 1 h and 2 h, respectively. At the same time, the amount of Ta is increasing apparently according to their XRD patterns. The morphology of the sample reduced for 0.5 h is shown in Fig. 7a. Some of the particles are bigger than 5 μm. The EDX analysis were carried on for the regions where the larger particle of E and the smaller one of F are found with the molar ratios of Ta to Ca are 37:9 and 55:0, respectively. Therefore, the larger particle is probably $Ta_2O_5{\cdot}0.5CaO$, while the smaller one is Ta by considering of their XRD results as well. Fig. 7b is the SEM image of the sample reduced for 2 h. The amount of small nodular particles is increasing, which are probably metallic Ta. The bigger particles may be $Ta_2O_5{\cdot}2CaO$ or $Ta_2O_5{\cdot}4CaO$, whose particle size is smaller than that of $Ta_2O_5{\cdot}0.5CaO$ particles shown in Fig. 7a. The surface of the bigger particles has a terraced structure, and there are traces of disagglomeration of $Ta_2O_5{\cdot}0.5CaO$ to $Ta_2O_5{\cdot}4CaO$ by combination of CaO. Fig. 6d–e shows the typical XRD patterns for the samples reduced for 6.5 h and 12 h, respectively. The major phases in the sample for 6.5 h are Ta and $Ta_2O_5{\cdot}4CaO$. There are also some typical peaks for $CaCO_3$, and its formation can be explained as mentioned previously.

After 12 h electrolysis, the starting material, Ta_2O_5 is completely reduced to Ta according to its XRD pattern. Its morphology is shown in Fig. 7c. The tantalum product consists of the interconnected nodular shape particles. It is intriguing that the particle size of most nodules is bigger than that of the particles reduced in the melt with the CaO concentration of 1 mol% higher. The reason is probably related with the role which CaO plays during electro-deoxidation. Suzuki and co-workers [4,13] had also found that CaO concentration affects the morphology of the tantalum powder, which is the product of calciothermic reduction of Ta_2O_5 in the molten $CaCl_2$.

Fig. 8 is the current vs. time curve of electrochemical reduction experiment in the $CaCl_2$–NaCl melt, in which cathode composition was given for various points in time during electrolysis. Its shape is somewhat different to that for the $CaCl_2$–NaCl with 1 mol% CaO, and the time-averaged current intensity for the first 5 h is lower, although the intermediate products of the electrochemi-

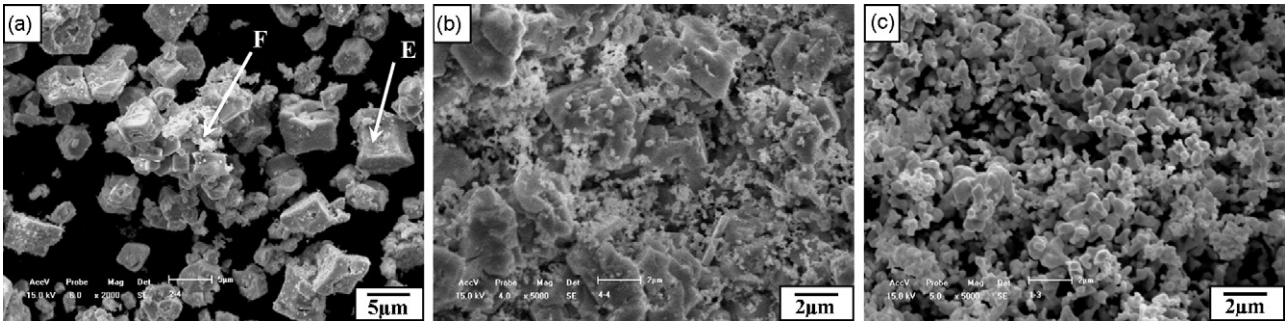

Fig. 7. SEM images of the samples electro-deoxidized in the $CaCl_2$–NaCl melt for (a) 0.5 h, (b) 2 h and (c) 12 h, respectively.

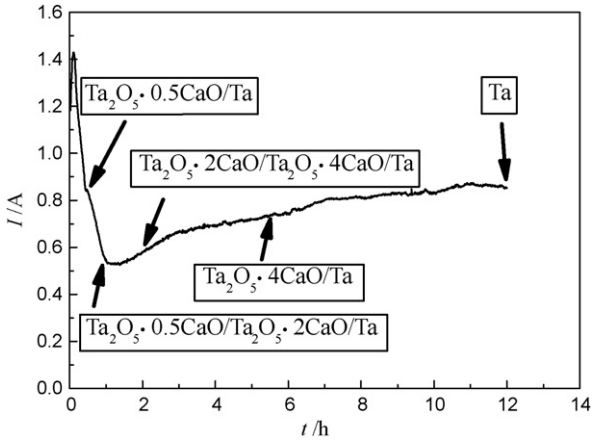

Fig. 8. The current vs. time curve of electrochemical reduction experiment in the $CaCl_2$–NaCl melt in which cathode composition was given for various points in time during electrolysis.

cal reductions are the same. This means CaO in the melt probably has some activation for the electrochemical reduction on the Ta_2O_5 cathode.

From the experimental results of this study, the driving-force of the incorporation of CaO into Ta_2O_5 should be the minimum of total chemical potential energy since calcium tantalates can be formed from Ta_2O_5 and CaO in the melt without any cathodic polarization. There is no evidence to confirm calcium tantalates as the products of the calcium cathodic intercalation, which was used to explain the formation of calcium titanates [20,21,33]. CaO in the $CaCl_2$–NaCl melt is incorporated with Ta_2O_5 to higher tantalates, such as Ta_2O_5·0.5CaO and Ta_2O_5·CaO, both having a much larger particle size, and Ta_2O_5·0.5CaO is the overwhelming phase for the sample which is simply immersed in the $CaCl_2$–NaCl melt. When the bulk concentration of CaO was increased by adding about 1 mol% CaO to the $CaCl_2$–NaCl melt, the major phases were Ta_2O_5·CaO and Ta_2O_5·2CaO, and the particle size of Ta_2O_5·2CaO is smaller than that of Ta_2O_5·CaO particles as shown in Fig. 1b. This implies incorporation of more CaO per Ta_2O_5 unit disintegrated the large grains of higher calcium tantalates, and this view was confirmed by the fact of the much smaller particle size of Ta_2O_5·4CaO. It means that CaO in the melt is a network modifier for the higher calcium tantalates with a larger particle size, which can be disintegrated to smaller ones, just like "hydration process" for ions in aqueous solutions. So, the higher the bulk concentration of CaO in the melt, the more opportunities for the higher tantalates to be separated to the lower ones with smaller particle size, which may strongly affect the particle size of the finally reduced product, metal tantalum.

4. Conclusions

The reaction pathway of electrochemical reduction of Ta_2O_5 to tantalum was studied under a voltage of 2.8 V in the $CaCl_2$–NaCl melt with and without the addition of CaO by interrupting the reduction after various reaction times at 1123 K. During the reduction process from Ta_2O_5 to Ta, the tantalum oxide cathode undergoes several intermediate phases, such as Ta_2O_5·0.5CaO, Ta_2O_5·2CaO, Ta_2O_5·4CaO, and finally changes to metal Ta. The incorporation of more CaO can disintegrate the higher calcium tantalates with a larger particle size to the lower ones with smaller particle size. The bulk concentration of CaO in the $CaCl_2$–NaCl melt seems to affect the particle size of the final product, Ta. The sintered porous Ta_2O_5 pellets can chemically react with CaO in the melt and form Ta_2O_5·nCaO, successively, in which n is strongly dependent on the concentration of CaO in the melt.

Acknowledgements

The authors acknowledge the National Natural Science Foundation of China (Grant No. 50574025 and 50374030), and the Natural Science Foundation of Liaoning Province (Grant No. 20062020), China, for financial support. The authors gratefully thank the financial support from the Ministry of Science and Technology of China (Grants No. 2007CB613801). The authors appreciate that Professor Fray Derek for critically reading the manuscript.

References

[1] I. Park, T.H. Okabe, Y. Waseda, J. Alloys Compd. 280 (1998) 265.
[2] T. Wu, X.B. Jin, W. Xiao, X.H. Hu, D.H. Wang, G.Z. Chen, Chem. Mater. 19 (2007) 153.
[3] S.M. Jeong, H.Y. Yoo, J.M. Hur, C.S. Seo, J. Alloys Compd. 440 (2007) 210.
[4] M. Baba, R.O. Suzuki, J. Alloys Compd. 392 (2005) 225.
[5] M. Baba, Y. Ono, R.O. Suzuki, J. Phys. Chem. Solids 66 (2005) 466.
[6] G.Z. Chen, D.J. Fray, T.W. Farthing, Nature 407 (2000) 361.
[7] D.J. Fray, T.W. Farthing, G.Z. Chen, International Patent PCT/GB99/01781.
[8] X.F. Hu, Q. Xu, Acta Metall. Sinica 42 (2006) 285.
[9] T.H. Okabe, I. Park, K.T. Jacob, J. Alloys Compd. 288 (1999) 200.
[10] B. Yuan, T.H. Okabe, J. Alloys Compd. 454 (2008) 185.
[11] T.H. Okabe, N. Sato, Y. Mitsuda, S. Ono, Mater. Trans. 44 (2003) 2646.
[12] T.H. Okabe, S. Iwata, M. Imagunbai, Mater. Jpn. (Bull. Jpn. Inst. Met.) 43 (2004) 34.
[13] R.O. Suzuki, M. Baba, Y. Ono, K. Yamamoto, J. Alloys Compd. 389 (2005) 310.
[14] H.H. Nersisyan, J.H. Lee, S.I. Lee, C.W. Won, Combust. Flame 135 (2003) 539.
[15] C.Y. Chen, X.G. Lu, Q. Li, H.W. Cheng, Rare Met. Mater. Eng. 36 (2007) 1991.
[16] C.Y. Chen, X.G. Lu, Acta Metall. Sinica 44 (2008) 145.
[17] X.Y. Yan, D.J. Fray, Metall. Trans. Trans. B 33B (2002) 685.
[18] X.Y. Yan, D.J. Fray, Adv. Funct. Mater. 15 (2005) 1757.
[19] G.Z. Chen, E. Gordo, D.J. Fray, Metall. Mater. Trans. B 35B (2004) 223.
[20] C. Schwandt, D.J. Fray, Electrochim. Acta 51 (2005) 66.
[21] D.T.L. Alexander, C. Schwandt, D.J. Fray, Acta Mater. 54 (2006) 2933.
[22] G.H. Qiu, D.H. Wang, X.B. Jin, G.Z. Chen, Electrochim. Acta 51 (2006) 5785.
[23] Q. Xu, L.Q. Deng, Y. Wu, T. Ma, J. Alloys Compd. 396 (2005) 288.
[24] T. Wu, W. Xiao, X. Jin, C. Liu, D.H. Wang, G.Z. Chen, Phys. Chem. 10 (2008) 1809.
[25] X.F. Hu, Q. Xu, Y. Wu, Mater. Rev. 19 (2005) 97.
[26] C. Schwandt, D.T.L. Alexander, D.J. Fray, Electrochim. Acta 54 (2009) 3819.
[27] X.Y. Yan, D.J. Fray, J. Appl. Electrochem. 39 (2009) 1349.
[28] B. Jackson, M. Jackson, D. Dye, D. Inman, J. Electrochem. Soc. 155 (2008) E171.
[29] S. Tan, T. Oers, M.K. Aydinol, T. Ozturk, I. Karakaya, J. Alloys Compd. 475 (2009) 368.
[30] B.J. Zhao, L. Wang, L. Dai, G.H. Cui, H.H. Zhou, R.V. Kumar, J. Alloys Compd. 468 (2009) 379.
[31] Y. Zhu, D.H. Wang, M. Ma, X.H. Hu, X.B. Jin, G.Z. Chen, Chem. Commun. 24 (2007) 2515.
[32] X. Kang, Q. Xu, S.J. Ma, L.N. Zhao, Q.S. Song, Electrochemistry 77 (2009) 663.
[33] K. Jiang, X.H. Hu, M. Ma, D.H. Wang, G.H. Qiu, X.B. Jin, G.Z. Chen, Angew. Chem. Int. Ed. 45 (2006) 428.
[34] G.Z. Chen, D.J. Fray, J. Electrochem. Soc. 149 (2002) E455.
[35] P. Kar, J.W. Evans, Electrochim. Acta 53 (2008) 5260.
[36] P. Kar, J. Solid State Electrochem. 12 (2008) 1611.
[37] M. Sales, G. Eguia, P. Quintana, L.M. Torres-Martinez, A.R. West, J. Solid State Chem. 143 (1999) 62.
[38] X.Y. Yan, D.J. Fray, J. Electrochem. Soc. 152 (2005) D12.
[39] X.Y. Yan, D.J. Fray, J. Electrochem. Soc. 152 (2005) E308.